

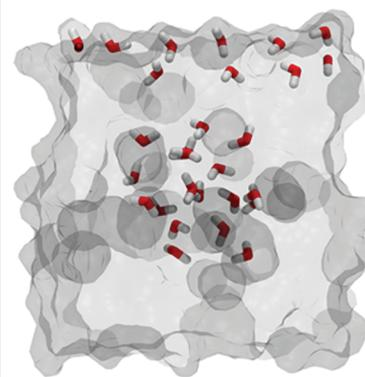
New Insights into the Structure of the Vapor/Water Interface from Large-Scale First-Principles Simulations

Thomas D. Kühne,^{*,†,‡} Tod A. Pascal,[§] Efthimios Kaxiras,[‡] and Yousung Jung^{*,§}

[†]Institute of Physical Chemistry and Center of Computational Sciences, Johannes Gutenberg University Mainz, Staudinger Weg 9, D-55128 Mainz, Germany, [‡]Department of Physics, and School of Engineering and Applied Sciences, Harvard University, Cambridge, Massachusetts 02138, United States, and [§]Graduate School of EEWS (WCU), Korea Advanced Institute of Science and Technology (KAIST), Daejeon 305-701, Korea

ABSTRACT We present extensive *ab initio* simulations of the molecular arrangements at the vapor/water interface, which provide valuable insights into the interface structure. In particular, the simulations address the controversy of whether there is a significant amount of nondonor configurations at this prototypical interface, using a novel Car–Parrinello-like *ab initio* molecular dynamics approach. The interface is modeled by a system of 384 water molecules for 125 ps in a two-dimensional periodic slab, the most extensive *ab initio* molecular dynamics simulation to date. In contrast to previous theoretical simulations and X-ray absorption spectroscopy, but consistent with sum-frequency generation experiments, we observe no evidence for a significant occurrence of acceptor-only species at the vapor/water interface. Besides a distinct surface relaxation effect, we find that only the topmost layers of the interface obey structural order.

SECTION Molecular Structure, Quantum Chemistry, General Theory



Many interesting chemical processes and phenomena in biology and chemistry often occur at aqueous hydrophobic interfaces.¹ Solvation, a central theme in protein folding,² electrochemical processes of aqueous batteries,³ and the remarkable organic catalysis “on water”^{4,5} are examples where studying the structure and dynamics of the corresponding aqueous interfaces is essential for the understanding of the relevant interfacial chemistry. The simplest and extreme case of an aqueous hydrophobic interface is the vapor/water interface, where there is no attractive or repulsive van der Waals force between the water and the hydrophobic phase. Because of its prototypical character, this particular interface has been studied extensively, both experimentally^{6–9} and theoretically.^{10–15} Understanding the air/water interface is very important for its relevance in atmospheric chemistry that occurs on the ice surface of dust particles or the ocean surface.^{16,17} Recently, it was suggested that the organic “on water” green catalysis is due to the free OH bonds of water molecules at the hydrophobic aqueous interface,⁵ a focus of the present paper.

The surface-specific vibrational sum-frequency generation (SFG) technique provided the first molecular picture of water at the air/water interface.¹⁸ About 25% of the surface water molecules have one dangling (or free) OH bond, which protrudes out of the water phase, consistent with earlier theoretical predictions.¹⁹ Similarly, dangling OH bonds have been consistently observed in other SFG experiments,^{7–9,20} but also in computer simulations.^{10–15} However, different interpretations were provided by others concerning structural and physical details of the air/water interface, in particular with respect to dangling OH groups.^{21,22}

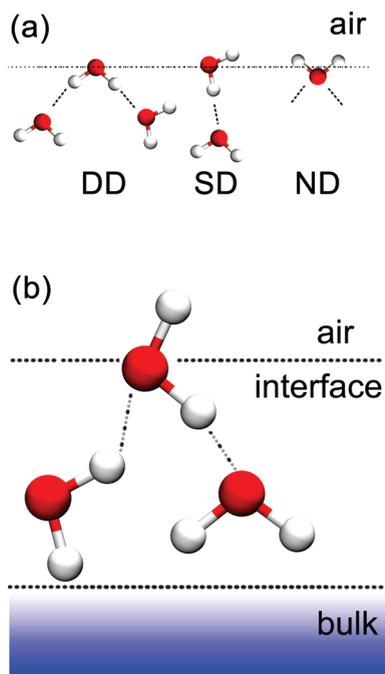
Depending on the number of OH groups per water molecule that forms a hydrogen (H) bond with another water molecule, we refer to them as double-donor (DD), single-donor (SD), and non-donor (ND)²¹ or “acceptor-only” configuration (Scheme 1a). In this notation, perfect crystalline bulk ice would have 100% DD configurations, in analogy to the tetrahedral textbook structure of liquid water and ice, while the (0001) basal plane of the defect-free hexagonal ice surface bilayer would have 25% SD and 75% DD configurations. In the latter ideal ice Ih surface, the probability of free OH bonds is identical to that of free oxygen lone pairs, both sticking out of the water phase. On the other hand, bulk liquid water and its surface are expected to have a mixture of ND, SD, and DD species with, on average, varying ratios caused by dynamic distortions of the liquid water H-bond network due to finite temperature. For instance, in bulk water, the probability of an OH bond being free (F_B) was estimated at 0.15, based on the experimental heat of melting of ice, which is 15% of the sublimation energy of ice.²³ For the air/water interface, the surface composition of the water configurations was given by Du et al.¹⁸ through “titrating” the dangling OH groups with methanol, followed by the observation of complete suppression of the free OH peak at 3700 cm^{-1} in the SFG measurements. From this, the authors estimated that the air/water interface consists of 25% SD and 75% DD water configurations

Received Date: October 11, 2010

Accepted Date: December 26, 2010

Published on Web Date: December 30, 2010

Scheme 1. (a) Depiction of Double Donor (DD), Single Donor (SD), and Non-donor (ND) Water Orientations at Air–Water Interface^a; (b) Schematic of Structure of Water Molecules near the Air–Water Interface from Our Ab Initio MD Simulations^b.



^aHydrogen bonding is indicated as dashed-dotted lines.^bSee also Figure 5.

yielding $F_s = 0.25$, similar to the (0001) ice Ih surface, except for the disordered nature of the liquid.

Recently, Cappa et al.²⁴ performed total ion yield (TIY) and total electron yield (TEY) X-ray absorption (XAS) measurements for the air/water interface and showed that the TIY-XAS (a surface probe) is nearly identical to the TEY-XAS (a bulk probe). The authors also indicated that in earlier measurements of the same group,²¹ where “the TIY-XAS of the air/water interface was similar to that of the gas-phase water (instead of bulk water)”, the gas phase contribution was not properly subtracted. The latter experimental artifact and corresponding DFT calculations of the XAS spectra on a rather small water cluster²¹ led those authors to suggest that they may have observed a new population of ND species of the air/water interface. For the related CCl_4 /water liquid/liquid interface, Scatena et al.²⁵ also suggested an interfacial water structure that involves a significant ND population based on the SFG measurements and their spectral decomposition of the free OH peak at 3700 cm^{-1} into the symmetric and antisymmetric OH vibrations, since the ND species, if populated, would exhibit two split peaks at around 3650 and 3750 cm^{-1} . However, such a splitting or a measurable population of ND species has not been observed in other SFG measurements and analyses of the air/water or organic/water interfaces.⁶ Even though these experiments are very powerful, it would be still desirable to directly observe the liquid/vapor interface and gain an atomistic understanding using molecular dynamics (MD) simulations. In this way, it is for

instance possible to extract the average population of ND, SD, and DD species and hence determine F as the weighted average of ND and SD configurations.

From a computational point of view, simulations of water are particularly challenging due to nonadditive cooperative effects of the H-bonded network, as well as large polarizability, dipole moment, and nuclear quantum effects, which make water unique.²⁶ The predictive power of such simulations critically depends on the involved time and length scales, to reduce statistical uncertainties and to eliminate finite-size effects, but also on the accuracy of the interaction potentials used. Since empirical potentials are typically parametrized to reproduce bulk rather than interfacial properties of liquid water, such as experimental energies, densities, pair-correlation functions and in some cases diffusion and dielectric constants, the transferability of empirical force fields can not be assured. Therefore, a first-principles approach such as density functional theory (DFT)-based ab initio MD (AIMD), where the interatomic forces are calculated “on-the-fly” by accurate electronic structure methods, is particularly appropriate for the study of interfaces involving water.

Even AIMD has its own restrictions, namely, that the increase in predictive power comes at the price of substantially higher computational cost. This becomes more problematic for the liquid/vapor interface where a system larger than those representing bulk features must be considered in order to stabilize a two-dimensional (2D) periodic water slab with a sufficiently large vacuum portion to prevent spurious long-range interactions at the surface. For this reason, it is not surprising that only recently a landmark effort using first-principles approaches has been reported by Kuo and Mundy.²² Although their observation of “acceptor-only” or ND moieties were in good agreement with the earlier experimental data of Wilson et al.,²¹ they are in contrast with the revised results of the Saykally group.²⁴ In addition, a recent study, although on a small water cluster rather than the more relevant vapor/water interface, suggested that the population of ND species at the “air/water interface” is very small.²⁷ Thus the question of whether a non-negligible fraction of ND water configurations exists at the vapor/water interface is at present controversial, with experimental and theoretical studies suggesting both possibilities.

Here, we use a novel AIMD simulation method, which is very accurate but at the same time at least 1 order of magnitude more efficient than previous approaches, to address this controversial issue. We elucidate the orientational structure of water at the vapor/water interface, as well as the structure of the corresponding H-bond network. These structural effects are shown to be directly related to the dielectric properties at the interface. To the best of our knowledge, our work represents the most extensive AIMD simulation to date.

The liquid water density of the vapor/liquid interface as a function of the z -coordinate is given in Figure 1. This density profile is fitted to the usual hyperbolic tangent function given as

$$\rho(z) = a \left(1 + \tanh \left(-\frac{z - z_G}{\delta} \right) \right) \quad (1)$$

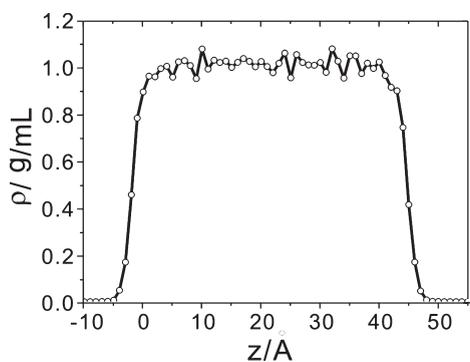


Figure 1. Density profile of the calculated water slab.

Table 1. Thickness Parameter (δ) of the Interface and the Bulk Density for Various Water Models

	BOMD/BLYP-D (this work)	CPMD/ BLYP ²²	Dang & Chang ³²	TIP4P-FQ ³¹
δ (Å)	1.71	0.78	1.45	1.58
Bulk density (g/cm ³)	1.01 ^a	0.86	0.98	1.01

^aThe density of water in the region $10 \text{ \AA} < z < 35 \text{ \AA}$ in Figure 1.

with the Gibbs dividing surface, i.e., the location where the average density equals 50% of the bulk density, denoted by z_G , while δ is a thickness parameter in the fitting. In this expression, $a = 0.505 \text{ g/mL}$, $z_G = 44.6 \text{ \AA}$, and $\delta = 1.71 \text{ \AA}$ ($a = 0.506 \text{ g/mL}$, $z_G = -1.838 \text{ \AA}$, and $\delta = 1.53 \text{ \AA}$ for the other side). If the interface is defined as usual to be the region where the density drops from 90% of the bulk density to 10%, here denoted using the notation [90, 10], the interfacial thickness $\Delta = 2.197\delta = 3.8 \text{ \AA}$. In connection with the surface specific SFG selection rule, where there will be signals whenever a net orientational ordering is present, in this work we define the approximate interfacial region to be [95, 5], or $z_G \pm 1.5\delta$. The bulk region is defined as $10 \text{ \AA} < z < 35 \text{ \AA}$ based on visual inspection of the density profile shown in Figure 1. Although we always considered both sides of the slab and confirm their consistency in the remainder of the paper, we report here only on interfacial properties for the upper side.

In Table 1, we compare the thickness parameter and the bulk density of water for various water models. Since it is well-known that the inclusion of van der Waals interactions systematically improves the density of liquid water,^{28,29} we have augmented our calculations by an empirical dispersion correction term.³⁰ In this way, we obtain a bulk water density of 1.01 g/cm^3 , which is in excellent agreement with the experimental value of 0.98 g/cm^3 . In particular, it is higher than the 0.86 g/cm^3 reported by Kuo and Mundy,²² which was obtained using the standard BLYP functional. Those authors also observe a much smaller interface thickness (0.78 \AA) than found in the current calculation (1.71 \AA), which is also closer to the results based on empirical but polarizable water models ($1.45\text{--}1.78 \text{ \AA}$).^{31,32} We wish to note that the bulk water density we observe is sustained for the whole length of the trajectory, which suggests the absence of a glassy state in liquid water in agreement with earlier calculations.³³

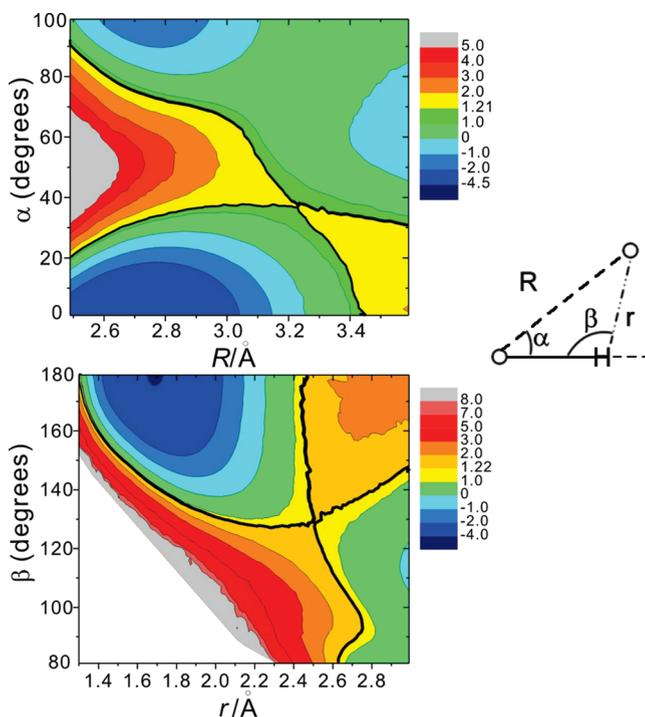


Figure 2. 2D-PMF-based H-bond definitions. Definitions of the water configurations are also shown by the schematic picture on the right. All distances are in Å. The contours are in units of $k_B T$, and the black lines define the surfaces passing through the saddle point, $1.21 k_B T$ and $1.22 k_B T$, respectively, for (R, α) and (r, β) combinations.

Energetic or geometric criteria are often used to determine whether a pair of water molecules are H-bonded or when a H-bond is broken, in order to facilitate the discussion of experimental and theoretical results. Since the distribution of water–water H-bonds is continuous, the sharp division of conventional H-bond definitions is arbitrary, and any analysis based on this arbitrary division would be affected by the H-bond parameter chosen. Therefore, contrary to the fixed distance-only or fixed distance–angle pair definitions typically used in the literature, we use the radial-angle joint distribution function and the potential of mean force (PMF) calculated from it, as suggested by Kumar et al.³⁴ This H-bond definition is parameter-free. Specifically, an equipotential region of the 2D PMF surface that passes through the saddle point and encircles the minimum is considered to be the H-bonded state, while all other combinations of (R, α) are considered to be H-bond broken or free OH bonds. In Figure 2, for example, two water molecules are regarded as H-bonded if their relative distance and orientation (R, α) are within the solid line encircling the minimum of this 2D-PMF plot. Using this construction scheme, we have created custom H-bond definitions for the bulk and the interface region. Alternatively, it is also possible to construct H-bond definitions with respect to different pairs, such as (r, β) , as shown in Figure 2.

For theoretical estimates of F and the average number of H-bonds per water molecule (n_{HB}), we decompose the H-bond configurations for the bulk as well as for the interface into the ND, SD, and DD species using various H-bond definitions.

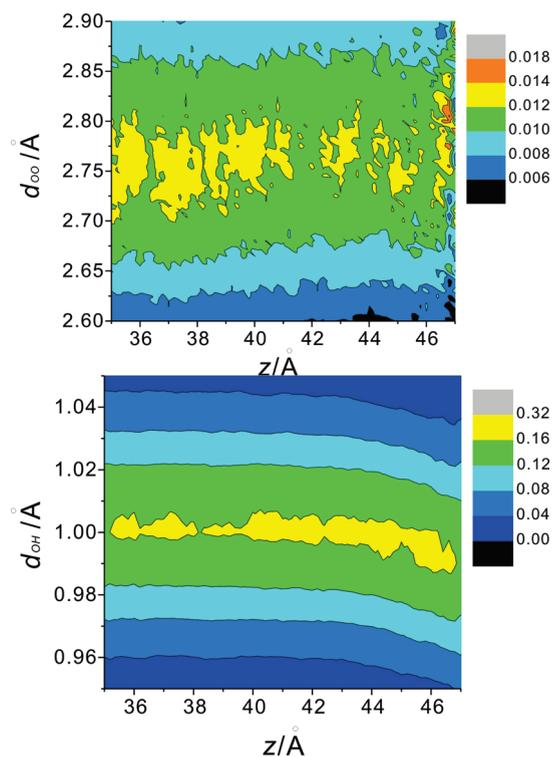
Table 2. Populations of the DD, SD, and ND Configurations of Water Molecules in the Bulk and at the Interface^a

	2D PMF (R, α)		2D PMF (r, β)		Wick et al, ref 32 ($r < 2.27 \text{ \AA}, \beta > 150^\circ$)		Kuo & Mundy, ref 22 ($r < 2.27 \text{ \AA}, \beta > 140^\circ$)		heat of melting data (ref 23)	SFG experiment (ref 35)
	bulk	surface	bulk	surface	bulk	surface	bulk	surface	bulk	surface
DD	0.84	0.49	0.84	0.48	0.42	0.30	0.40	0.14		
SD	0.15	0.45	0.15	0.45	0.48	0.56	0.45	0.66		
ND	0.01	0.06	0.01	0.07	0.08	0.14	0.12	0.19		
F (free OH)	0.08	0.29	0.08	0.29	0.32	0.42	0.35	0.52	0.15	0.25
$\langle n_{\text{HB}} \rangle$	3.7	2.9	3.7	2.8	2.7	2.4	2.5	1.9	3.4	3.0

^a When we use the H-bond definition in ref 22 ($r < 2.27 \text{ \AA}, \beta > 140^\circ$) for the present ab initio trajectory, we obtain ND = 0.10, SD = 0.43, and DD = 0.47 for bulk water ($\langle n_{\text{HB}} \rangle_{\text{B}} = 2.77$), and ND = 0.21, SD = 0.52, and DD = 0.27 for surface ($\langle n_{\text{HB}} \rangle_{\text{S}} = 2.13$). With the fixed definition ($r < 2.27 \text{ \AA}, \beta > 150^\circ$) in ref 32, we obtain ND = 0.05, SD = 0.33, and DD = 0.62 for bulk water ($\langle n_{\text{HB}} \rangle_{\text{B}} = 3.12$), and ND = 0.14, SD = 0.50, and DD = 0.36 for surface ($\langle n_{\text{HB}} \rangle_{\text{S}} = 2.44$).

The corresponding results are summarized in Table 2. Both of our 2D-PMF-based H-bond definitions give very similar results for bulk water, where the tetrahedral DD configuration is the dominant species, with about 84%, which results in $F_{\text{B}} \approx 0.08$ and $\langle n_{\text{HB}} \rangle_{\text{B}} \approx 3.7$. These theoretical estimates yield a bulk water structure that is somewhat more crowded as compared to the experimental estimates, $F_{\text{B}}(\text{exp}) \approx 0.15$ and $\langle n_{\text{HB}} \rangle_{\text{B}}(\text{exp}) = 3.4$.²³ Using the corresponding PMF-based H-bond definitions, the interface consists of approximately 50% DD, 45% SD, and 5% ND species, which gives $F_{\text{S}} \approx 0.29$ and $\langle n_{\text{HB}} \rangle_{\text{S}} \approx 2.8$, respectively. The values of F_{S} and $\langle n_{\text{HB}} \rangle_{\text{S}}$ are close to the experimentally observed fraction of surface water molecules that have one free OH bond, i.e., $F_{\text{S}}(\text{exp}) = 0.25$ and $\langle n_{\text{HB}} \rangle_{\text{S}}(\text{exp}) = 3.0$, from SFG measurements.³⁵

However, the computed fraction of interfacial ND species using our PMF-based H-bond definitions of the present study (6–7%) is, by a factor of 2–3, substantially smaller than the previous theoretical estimates of Kuo and Mundy^{22,32} (14–19%). In other words, our current AIMD results do not support the conjecture of a significant population of ND species at the vapor/water interface. By further inspection, we find that the theoretical results in ref 22 yield $F_{\text{S}} \approx 0.52$, which is more than twice as large as the SFG derived fraction of 0.25 or the present AIMD result $F_{\text{S}} \approx 0.29$, which immediately suggests that the liquid water surface is somewhat less reactive than proposed. Furthermore, since for bulk water $\langle n_{\text{HB}} \rangle_{\text{B}} \approx 2.5$ – 2.7 in ref 22, which is not only smaller than the experimental value $\langle n_{\text{HB}} \rangle_{\text{B}} \approx 3.4$, but would also be incompatible with the traditional tetrahedral picture of liquid water, we find it suggestive to attribute the deviation to a too restrictive H-bond definition, whose parameters were chosen to sample the experimentally determined hydrogen bond population within arbitrarily chosen 4σ of the distance distribution.²² In fact, the importance of the particular H-bond definition on the population of the various species at the liquid/vapor interface is well-known.³¹ Using the same H-bond definition as in ref 22 and a surface thickness of $|z_{\text{int}}| \geq z_{\text{S}} - 2 \text{ \AA}$, we find that for the liquid/vapor interface the fraction of ND configurations increases from 6–7% to 21% (Table 2) using AIMD trajectories from the present simulations. Also, the higher bulk water density of the present AIMD simulation (1.01 g/cm³ vs 0.86 g/cm³) is another possible cause for the different surface structures.


Figure 3. Average OO and intramolecular OH distances as a function of the depth position z (all distances in Å).

The average oxygen–oxygen distance is typically increased at the interface, compared to bulk water.²⁶ In fact, an expansion by about 6% has been observed in recent extended XAS fine structure experiments.³⁶ Instead, most empirical water models, polarized or not, such as TIP4P, TIP4P-POL2, and TIP4P-FQ, all predicted a shortening of the average O–O distance except for the Dang–Chang model, which predicts an expansion by 0.01 Å (<0.5%).³¹ On the other hand, DFT-based CPMD calculations predict an expansion of 0.03 Å (1%).^{31,32} In Figure 3, we plot the average O–O distance distributions of the H-bonded water molecules as a function of the z -coordinate.

The current simulation predicts a similar elongation to previous DFT calculations, that is, an increase in the O–O

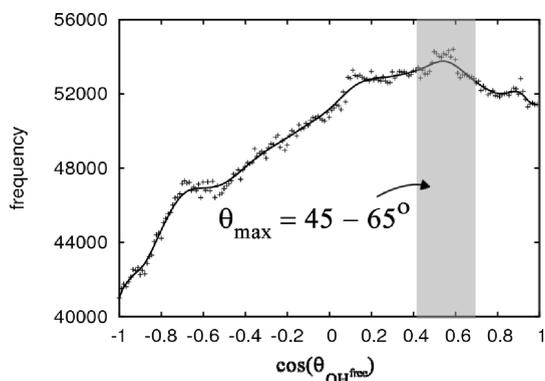


Figure 4. Orientational distribution of free OH bonds $P(\cos \theta_{\text{OH}})$ as a function of the tilt angle θ_{OH} using the 2D-PMF-based H-bond definition and an interfacial thickness defined as $z_G \pm 1.5\delta$.

distance by about 0.02 \AA ($< 1\%$). Even though it may be desirable to re-examine the extent of the surface relaxation effect using hybrid functionals that include at least partially Hartree–Fock exchange³⁷ or nuclear quantum effects,³⁸ at this point we can not confirm an O–O expansion that is as large as 6%. Incidentally, the same authors of ref 36 have lately revisited the TiY-XAS spectra of liquid water and suggested a potential reconsideration of earlier EXAFS measurements whose quantitative analysis yielded an OO distance increase of 6% at the liquid water interface.²⁴ Therefore, not just theoretically, but also experimentally revisiting this question may be helpful.

A partial orientational ordering of water molecules occurs at the vapor/water interface, with free OH bonds preferentially protruding out of the water toward the vapor phase. Experimentally, the orientation of free OH bonds at the vapor/water interface has been deduced from SFG measurements by assuming a particular form for the orientational distribution function.⁹ Typically, either Gaussian or Heaviside step functions are used, which yield $\langle \theta_{\text{OH}} \rangle \approx 30\text{--}35^\circ$, where θ_{OH} is the angle between the free OH bond and the surface normal. In contrast to these experimental interpretations, most previous MD simulations with various water models predicted an average tilt angle that is considerably closer to the plane of the surface, ranging between $\langle \theta_{\text{OH}} \rangle = 60$ and 80° . The determination of the experimental $\langle \theta_{\text{OH}} \rangle$ from SFG depends on some assumptions and approximations involved in the analysis. Likewise, the computational estimates depends on the definition of the interfacial thickness, the H-bond definition used in the analysis, as well as the particular empirical or first-principles water potential.

In Figure 4, we plot the orientational distribution of free OH bonds $P(\cos \theta_{\text{OH}})$ as a function of the tilt angle θ_{OH} using the 2D-PMF-based H-bond definition and an interfacial thickness defined as $z_G \pm 1.5\delta$. We smooth the data with a cubic spline function (solid line) for presentation purposes. We use equal weights for all surface layers when calculating the orientational distribution function and tilt angle average. The maximum of the broad distribution occurs at $45\text{--}65^\circ$ with an average of 56° . The distribution shown in Figure 4 is not well characterized by either a Heaviside or Gaussian function.

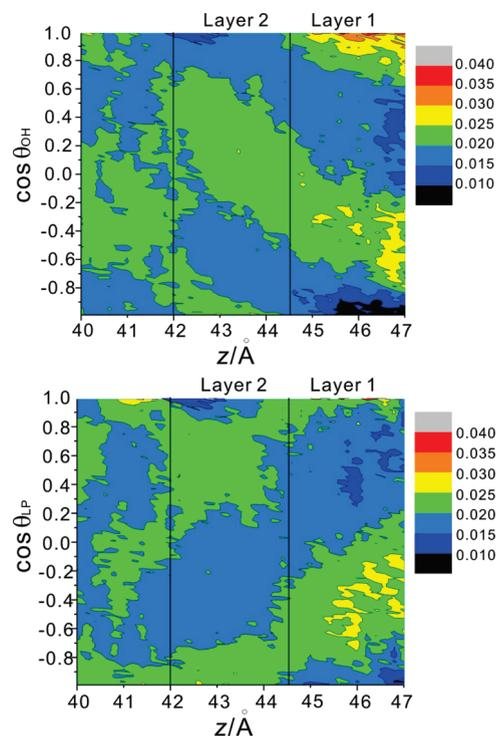


Figure 5. Orientational distribution of (a) all OH bonds and (b) lone pairs as a function of the depth position near the interface z (all distances in \AA).

To understand the H-bonded structure of water at the interfacial region, we separately analyzed the orientational distribution of all OH bonds (both free and H-bonded). They are plotted in Figure 5a. First of all, we find that only the two layers on top of the slab obey structural order. In the uppermost layer, the highest probability occurs for $\cos \theta_{\text{OH}} \sim 1 = 0^\circ$ and $-0.4 = 110^\circ$, which corresponds to OH bonds that are sticking out of the water into the vapor phase but also to OH bonds that are pointing toward the second subjacent layer. In this second layer, the maxima of the distribution function are antipodal to the first layer, i.e., the OH bonds tend to point on one hand into the bulk phase, but also toward the overlying layer.

Although the free OH bonds can be probed and interpreted in terms of their orientations using SFG, the free lone pairs (lone pairs that are not H-bonded to other water molecules) of oxygen are difficult to probe. For the latter lone pairs, computer simulations can particularly be helpful to understand whether the lone pairs may also have a preferential orientational ordering like free OH bonds. Therefore in Figure 5b, we plot $P(\cos \theta_{\text{LP}})$ for the lone pair electrons of oxygen at the interface. The lone pairs are assumed to form an angle of 104.5° and are located perpendicular to the HOH plane along the bisector of the HOH angle. A recent MD study with the fixed charge water models³⁹ indicated that the orientational ordering of the lone pairs depends strongly on the water model used, 3-, 4-, or 5-site models. Our ab initio calculations are not biased with such empirical structural models, and would suggest a more rigorous structural picture regarding the lone-pair orientations. As can be seen in Figure 5b, the present

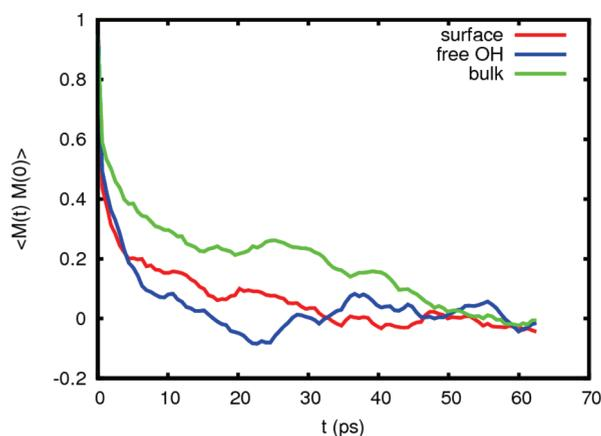


Figure 6. Molecular reorientation time of the bulk water, surface water, and the free OH bonds.

DFT calculations suggest that there is only a small probability of lone pair orbitals that protrude out of the first and second layers into the gas and bulk phase, respectively. However, at the same time there are probability maxima where lone pairs of the topmost layer are pointing into the second layer and vice versa. Among the empirical models tested in ref 39, the 3-site SPC/E model yields a lone pair orientation similar to that of the current DFT results. Combining the orientational ordering of OH bonds and the lone pairs of oxygen, a layered structure of water similar to the ice surface can be deduced, as in Scheme 1b.

Calculation of the molecular reorientation time is of particular interest, as it gives further information about the local environment and can be probed experimentally by dielectric relaxation (DR) techniques.⁴⁰ Indeed, critical understanding about the nature of water molecules at the surface of biological molecules, colloids, and hydrophobic solutes have arisen from these DR experiments.⁴¹ Computationally, the characteristic reorientation time τ is calculated as the integral of the dipole moment autocorrelation function $\varphi(t)$

$$\tau = \int \varphi(t) dt = \int \frac{\langle M(t) \cdot M(0) \rangle}{\langle M(0) \cdot M(0) \rangle} dt \quad (3)$$

where $M(t)$ is the total dipole moment and $\langle \dots \rangle$ represents the statistical ensemble average (see Figure 6).⁴² We use the fixed charges of the SPC water model when calculating the dipole moments. The method of Kuo et al.³¹ is employed to calculate the interfacial residence time, while the method of Impley et al.⁴³ is used to obtain the bulk residence time.⁴⁴ To that extent, we have only considered water molecules that either stayed in the particular region of interest for the entire 60 ps, or may have left that region but returned within 0.1 ps. The calculated residence times for the water molecules at the interface is 7.5 ps in comparison to 4.8 ps in the bulk for water molecules moving out of the first solvation shell.

Using eq 3, we find that the surface water molecules have a 3-fold smaller reorientation time than bulk water molecules, namely, 3.9 ps versus 11.5 ps, which is consistent with a prior ab initio MD simulation for which 1.5 ps of data were provided³¹ (versus more than 60 ps in the present work), as

well as simulations using classical forcefields.^{31,44} The reorientation time obtained for the bulk is a collective correlation time of the system⁴² and can be compared to the principal relaxation time of 8.32 ps for bulk liquid water obtained from DR measurements.^{45,46} Our value is about 40 % greater than experiment. Note that a molecular-level interpretation of this “collective relaxation” is still controversial and beyond the scope of this work.^{47,48} Meanwhile, our value of 3.9 ps obtained for the interface is more like a single-particle correlation time and can be compared to the molecular reorientation time of 2.1 ps at 300 K obtained from NMR measurements.⁴⁹ Perhaps due to a smaller average number of H-bonds at the interface, the surface orientational relaxation time of the water molecules is shorter than the one of bulk water. By analyzing only the ND and SD water molecules at the surface, we calculate a relaxation time of 2.6 ps, or 33 % less than the total from all surface water molecules. Those surface water molecules with at least one free OH bond have even shorter reorientation times than the average surface water molecules, most likely due to an even smaller number of H-bonds.

To summarize, in this work we used a novel Car–Parrinello-like approach that is very accurate, but at the same time at least 1 order of magnitude more efficient than previous algorithms, to study the vapor/water interface. By a now possible extensive sampling of the molecular configurations, we address the controversy of whether there is a significant amount of acceptor-only configurations at the vapor/water interface. In agreement with SFG measurements, but at variance to previous XAS experiments and AIMD simulations, we find no signature for a significant amount of acceptor-only configurations.

We also determined the tilt angle average of the free OH bonds normal to the interface to be $\langle \theta_{\text{OH}} \rangle = 56^\circ$, somewhat larger than the $30\text{--}35^\circ$ deduced from SFG measurements assuming a particular form of distribution such as delta, Gaussian, or Heavyside step functions for the orientational distribution function. Our computed distribution using first-principles calculations, however, is not characterized by any of the model functions, but is shown to be much broader.

Furthermore, we find that only the uppermost layers are structurally ordered. In this band close to the surface, we observed an expansion ($< 1\%$) of the average O–O distance as shown experimentally, even though to a much less distinct extent. The orientational relaxation time of the surface water molecules is much smaller than that of the bulk water molecules, most likely due to the smaller number of H-bonds at the interface. Surface water molecules with only dangling OH bonds reorient even faster than the rest of surface water molecules due to its “free” nature.

METHODS AND COMPUTATIONAL DETAILS

Since the direct Born–Oppenheimer MD (BOMD) approach, where the energy functional is fully optimized in every MD step, would have been prohibitive, we employ here the recently devised “Car–Parrinello-like approach to Born–Oppenheimer MD” of Kühne et al.,⁵⁰ which has already demonstrated its superior efficiency.⁵¹ In the spirit of the original Car–Parrinello MD (CPMD) scheme,⁵² during the

dynamics, the electronic wave functions are not self-consistently optimized. However, at variance to CPMD, in this approach the fictitious Newtonian dynamics of the electrons and ions is substituted by a similarly coupled electron-ion MD, which does not require the definition of a fictitious mass parameter, but at the same time keeps the electrons very close to their instantaneous electronic ground state. As a consequence, the time step can be chosen to be as large as the particular ionic resonance limit, while simultaneously preserving the efficiency of CPMD. By this means, the best aspects of the BOMD and CPMD methods are unified, which not only extends the scope of either method but allows for ab initio simulations previously thought to be unfeasible. The dynamics thus obtained is slightly dissipative of the type $-\gamma_D \dot{R}_I$, where R_I are the ionic coordinates. Reference 50 describes how to compensate for this dissipation by devising a modified Langevin equation and still obtain a correct canonical sampling of the Boltzmann distribution.

Our model of the liquid/vapor interface consists of a bulk water part with 384 light water molecules in an orthorhombic box of dimension $15.64 \times 15.64 \times 46.92 \text{ \AA}^3$ plus an additional vacuum along the surface direction subject to periodic boundary conditions (PBC). The simulations are performed in the canonical (NVT) ensemble at 300 K using an integration time step of $\Delta t = 0.5 \text{ fs}$.

Before starting the actual AIMD, the sample is prepared by equilibrating the bulk water part under three-dimensional (3D) PBC for 1.25 ns using the empirical SPC/Fw water potential in conjunction with the FIST module of CP2K.⁵³ Thereafter the interface is created by interfacing the bulk with 10 nm vacuum, before re-equilibrating it again for 1.25 ns.

The DFT-based AIMD simulation is conducted using a modified version of the mixed Gaussian and plane wave code⁵⁴ CP2K/Quickstep.⁵⁵ In this method, the Kohn–Sham orbitals are expanded in contracted Gaussians, whereas the electronic charge density is represented using plane waves. For the former, we use an accurate triple-basis set with two additional sets of polarization functions (TZV2P),⁵⁶ while for the latter we employ a density cutoff of 320 Ry. The unknown exchange and correlation potential is substituted by the BLYP-D generalized gradient approximation plus a damped interatomic potential to account for van der Waals interactions.⁵⁰ Because the system is disordered with a large band gap, the Brillouin zone is sampled at the Γ -point only. Interactions between the valence electrons and the ionic cores are described by norm-conserving pseudopotentials.^{57,58} The Poisson problem is tackled using an efficient Wavelet-based solver,⁵⁹ which allows for a rather small vacuum portion chosen to be 8 \AA on both sides along the nonperiodic direction. The parameter for the modified Langevin equation is adjusted to be $\gamma_D = 9.85 \times 10^{-5} \text{ fs}^{-1}$, while the electronic degrees of freedom are propagated as described in ref 60 ($K = 7$). Before statistics are eventually accumulated for 125 ps, the whole system is once again equilibrated for 25 ps.

AUTHOR INFORMATION

Corresponding Author:

*To whom correspondence should be addressed. E-mail: kuehne@uni-mainz.de (T.D.K.); ysjn@kaist.ac.kr (Y.J.).

ACKNOWLEDGMENT The generous allocation of computer time from the Harvard FAS Research Computing Group and the Swiss National Supercomputing Center (CSCS), as well as technical support from Neil Stringfellow is kindly acknowledged. It is also a pleasure to acknowledge the support by the WCU program (31-2008-000-10055-0) and Ministry of Education, Science, and Technology (NRF-2010-0029034) through the National Research Foundation of Korea.

REFERENCES

- (1) Ball, P. Water as an Active Constituent in Cell Biology. *Chem. Rev.* **2008**, *108*, 74–108.
- (2) Dobson, C. M. Protein Folding and Misfolding. *Nature* **2003**, *426*, 884–890.
- (3) Luo, J.-Y.; Cui, W.-J.; He, P.; Xia, Y.-Y. Raising the Cycling Stability of Aqueous Lithium-Ion Batteries by Eliminating Oxygen in the Electrolyte. *Nat. Chem.* **2009**, *2*, 760–765.
- (4) Narayan, S.; Muldoon, J.; Finn, M. G.; Fokin, V. V.; Kolb, H. C.; Sharpless, K. B. “On Water”: Unique Reactivity of Organic Compounds in Aqueous Suspension. *Angew. Chem., Int. Ed.* **2005**, *117*, 3339–3343.
- (5) Jung, Y.; Marcus, R. A. On the Theory of Organic Catalysis “on Water”. *J. Am. Chem. Soc.* **2007**, *129*, 5492–5502. Jung, Y.; Marcus, R. A. Protruding Interfacial OH Groups and “On Water” Heterogeneous Catalysis. *J. Phys.: Condens. Matter* **2010**, *22*, 284117.
- (6) Shen, Y. R.; Ostroverkhov, V. Sum-Frequency Vibrational Spectroscopy on Water Interfaces: Polar Orientation of Water Molecules at Interfaces. *Chem. Rev.* **2006**, *106*, 1140–1154.
- (7) Richmond, G. L. Molecular Bonding and Interactions at Aqueous Surfaces as Probed by Vibrational Sum Frequency Spectroscopy. *Chem. Rev.* **2002**, *102*, 2693–2724.
- (8) Gopalakrishnan, S.; Jungwirth, P.; Tobias, D. J.; Allen, H. C. Air–Liquid Interface of Aqueous Solutions Containing Ammonium and Sulfate: Spectroscopic and Molecular Dynamics Studies. *J. Phys. Chem. B* **2005**, *109*, 8861–8872.
- (9) Gan, W.; Wu, D.; Zhang, Z.; Feng, R.-R.; Wang, H.-F. Polarization and Experimental Configuration Analyses of Sum Frequency Generation Vibrational Spectra, Structure, and Orientational Motion of the Air/Water Interface. *J. Chem. Phys.* **2006**, *124*, 114705.
- (10) Dang, L. X.; Chang, T. M. Molecular Dynamics Study of Water Clusters, Liquid, and Liquid–Vapor Interface of Water with Many-Body Potentials. *J. Chem. Phys.* **1997**, *106*, 8149.
- (11) Morita, A.; Hynes, J. T. A Theoretical of the Sum Frequency Generation Spectrum of the Water Surface. *Chem. Phys.* **2000**, *258*, 371–390.
- (12) Buch, V. Molecular Structure and OH-Stretch Spectra of Liquid Water Surface. *J. Phys. Chem. B* **2005**, *109*, 17771–17774.
- (13) Mundy, C. J.; Kuo, I.-F. W. First-Principles Approaches to the Structure and Reactivity of Atmospherically Relevant Aqueous Interfaces. *Chem. Rev.* **2006**, *106*, 1282–1304.
- (14) Taylor, R. S.; Dang, L. X.; Garrett, B. C. Molecular Dynamics Simulations of the Liquid/Vapor Interface of SPC/E Water. *J. Phys. Chem.* **1996**, *100*, 11720–11725.
- (15) Perry, A.; Neipert, C.; Space, B.; Moore, P. B. Theoretical Modeling of Interface Specific Vibrational Spectroscopy: Methods and Applications to Aqueous Interfaces. *Chem. Rev.* **2006**, *106*, 1234–1258.
- (16) Mantz, Y. A.; Geiger, F. M.; Molina, L. T.; Molina, M. J.; Trout, B. L. First-Principles Theoretical Study of Molecular HCl Adsorption on a Hexagonal Ice (0001) Surface. *J. Phys. Chem. A* **2001**, *105*, 7037–7046.

- (17) Molina, M. J. *The Probable Role of Stratospheric Ice Clouds: Heterogeneous Chemistry of the Ozone Hole*; Blackwell Scientific Publications: Oxford, 1994.
- (18) Du, Q.; Superfine, R.; Freysz, E.; Shen, Y. R. Vibrational Spectroscopy of Water at the Vapor/Water Interface. *Phys. Rev. Lett.* **1993**, *70*, 2313–2316.
- (19) Lee, C.-Y.; McCammon, J. A.; Rossky, P. J. The Structure of Liquid Water at an Extended Hydrophobic Surface. *J. Chem. Phys.* **1984**, *80*, 4448.
- (20) Eisenthal, K. B. Liquid Interfaces Probed by Second-Harmonic and Sum-Frequency Spectroscopy. *Chem. Rev.* **1996**, *96*, 1343–1360.
- (21) Wilson, K. R.; Cavalleri, M.; Rude, B. S.; Schaller, R. D.; Nilsson, A.; Pettersson, L. G. M.; Goldman, N.; Catalano, T.; Bozek, J. D.; Saykally, R. J. Characterization of Hydrogen Bond Acceptor Molecules at the Water Surface Using Near-Edge X-ray Absorption Fine-Structure Spectroscopy and Density Functional Theory. *J. Phys.: Condens. Matter* **2002**, *14*, L221–L226.
- (22) Kuo, I.-F. W.; Mundy, C. J. An Ab Initio Molecular Dynamics Study of the Aqueous Liquid-Vapor Interface. *Science* **2004**, *303*, 658–660.
- (23) Pauling, L. *The Nature of the Chemical Bond*; Cornell University Press: Ithaca, NY, 1960.
- (24) Cappa, C. D.; Smith, J. D.; Wilson, K. R.; Saykally, R. J. Revisiting the Total Ion Yield X-ray Absorption Spectra of Liquid Water Microjets. *J. Phys.: Condens. Matter* **2008**, *20*, 205105.
- (25) Scatena, L. F.; Brown, M. G.; Richmond, G. L. Water at Hydrophobic Surfaces: Weak Hydrogen Bonding and Strong Orientation Effects. *Science* **2001**, *292*, 908–912.
- (26) Stillinger, F. H. Water Revisited. *Science* **1980**, *209*, 451–457.
- (27) Galamba, N.; Costa Cabral, B. J. The Changing Hydrogen-Bond Network of Water from the Bulk to the Surface of a Cluster: A Born-Oppenheimer Molecular Dynamics Study. *J. Am. Chem. Soc.* **2008**, *130*, 17955–17960.
- (28) Schmidt, J.; VandeVondele, J.; Kuo, I.-F. W.; Sebastiani, D.; Siepmann, J. I.; Hutter, J.; Mundy, C. J. Isobaric-Isothermal Molecular Dynamics Simulations Utilizing Density Functional Theory: An Assessment of the Structure and Density of Water at Near-Ambient Conditions. *J. Phys. Chem. B* **2009**, *113*, 11959–11964.
- (29) Mundy, C. J.; Kuo, I.-F. W.; Tuckerman, M. E.; Lee, H.-S.; Tobias, D. J. Hydroxide Anion at the Air–Water Interface. *Chem. Phys. Lett.* **2009**, *481*, 2–8.
- (30) Grimme, S. Semiempirical GGA-Type Density Functional Constructed with a Long-Range Dispersion Correction. *J. Comput. Chem.* **2006**, *27*, 1787–1799.
- (31) Kuo, I.-F. W.; Mundy, C. J.; Eggimann, B. L.; McGrath, M. J.; Siepmann, J. I.; Vieceli, J.; Tobias, D. J. Structure and Dynamics of the Aqueous Liquid–Vapor Interface: A Comprehensive Particle-Based Simulation Study. *J. Phys. Chem. B* **2006**, *110*, 3738–3746.
- (32) Wick, C. D.; Kuo, I.-F. W.; Mundy, C. J.; Dang, L. X. The Effect of Polarizability for Understanding the Molecular Structure of Aqueous Interfaces. *J. Chem. Theory Comput.* **2007**, *3*, 2002–2010.
- (33) Lee, H.-S.; Tuckerman, M. E. Dynamical Properties of Liquid from Ab-Initio Molecular Dynamics Performed in the Complete Basis Set Limit. *J. Chem. Phys.* **2007**, *126*, 164501.
- (34) Kumar, R.; Schmidt, J. R.; Skinner, J. L. Hydrogen Bonding Definitions and Dynamics in Liquid Water. *J. Chem. Phys.* **2007**, *126*, 204107.
- (35) Du, Q.; Freysz, E.; Shen, Y. R. Surface Vibrational Spectroscopic Studies of Hydrogen Bonding and Hydrophobicity. *Science* **1994**, *264*, 826–828.
- (36) Wilson, K. R.; Schaller, R. D.; Co, D. T.; Saykally, R. J.; Rude, B. S.; Catalano, T.; Bozek, J. D. Surface Relaxation in Liquid Water and Methanol Studied by X-ray Absorption Spectroscopy. *J. Chem. Phys.* **2002**, *117*, 7738–7744.
- (37) Guidon, M.; Schiffmann, F.; Hutter, J.; VandeVondele, J. Ab Initio Molecular Dynamics Using Hybrid Density Functionals. *J. Chem. Phys.* **2008**, *128*, 214104.
- (38) Morrone, J. A.; Car, R. Nuclear Quantum Effects in Water. *Phys. Rev. Lett.* **2008**, *101*, 017801.
- (39) Fan, Y.; Chen, X.; Cremer, P. S.; Gao, Y. Q. On the Structure of Water at the Aqueous/Air Interface. *J. Phys. Chem. B* **2009**, *113*, 11672–11679.
- (40) Nandi, N.; Bhattacharyya, K.; Bagchi, B. Dielectric Relaxation and Solvation Dynamics of Water in Complex Chemical and Biological Systems. *Chem. Rev.* **2000**, *100*, 2013–2046.
- (41) Pal, S.; Balasubramanian, S.; Bagchi, B. Anomalous Dielectric Relaxation of Water Molecules at the Surface of an Aqueous Micelle. *J. Chem. Phys.* **2004**, *120*, 1912.
- (42) Neumann, M. Dielectric Relaxation in Water. Computer Simulations with the TIP4P Potential. *J. Chem. Phys.* **1986**, *85*, 1567–1580.
- (43) Impey, R. W.; Madden, P. A.; McDonald, I. R. Hydration and Mobility of Ions in Solution. *J. Phys. Chem.* **1983**, *87*, 5071–5083.
- (44) Marti, J.; Guardia, E.; Gordillo, M. C. Reorientational Motions in Sub- and Supercritical Water Under Extreme Confinement. *Chem. Phys. Lett.* **2002**, *365*, 536–541.
- (45) Barthel, J.; Bachhuber, K.; Buchner, R.; Hetzenauer, H. Dielectric Spectra of Some Common Solvents in the Microwave Region. Water and Lower Alcohols. *Chem. Phys. Lett.* **1990**, *165*, 369–373.
- (46) Barthel, J.; Buchner, R. High Frequency Permittivity and Its Use in the Investigation of Solution Properties. *Pure Appl. Chem.* **1991**, *63*, 1473–1482.
- (47) Agmon, N. Tetrahedral Displacement: The Molecular Mechanism Behind the Debye Relaxation in Water. *J. Phys. Chem.* **1996**, *100*, 1072–1080.
- (48) Arkhipov, V. I. Hierarchy of Dielectric Relaxation Times in Water. *J. Non-Cryst. Solids* **2002**, *305*, 127–135.
- (49) Jonas, J.; DeFries, T.; Wilbur, D. J. Molecular Motions in Compressed Liquid Water. *J. Chem. Phys.* **1976**, *65*, 582–588.
- (50) Kühne, T. D.; Krack, M.; Mohamed, F. R.; Parrinello, M. Efficient and Accurate Car–Parrinello-like Approach to Born–Oppenheimer Molecular Dynamics. *Phys. Rev. Lett.* **2007**, *98*, 066401.
- (51) Caravati, S.; Bernasconi, M.; Kühne, T. D.; Krack, M.; Parrinello, M. Coexistence of tetrahedral- and octahedral-like sites in amorphous phase change materials. *Appl. Phys. Lett.* **2007**, *91*, 171906. Caravati, S.; Bernasconi, M.; Kühne, T. D.; Krack, M.; Parrinello, M. First-principles study of crystalline and amorphous Ge₂Sb₂Te₅ and the effects of stoichiometric defects. *J. Phys.: Condens. Matter* **2009**, *21*, 255501. Caravati, S.; Bernasconi, M.; Kühne, T. D.; Krack, M.; Parrinello, M. Unravelling the Mechanism of Pressure Induced Amorphization of Phase Change Materials. *Phys. Rev. Lett.* **2009**, *102*, 205502. Camellone, M. F.; Kühne, T. D.; Passerone, D. Density functional theory study of self-trapped holes in disordered SiO₂. *Phys. Rev. B* **2009**, *80*, 033205. Cucinotta, C. S.; Miceli, G.; Raiteri, P.; Krack, M.; Kühne, T. D.; Bernasconi, M.; Parrinello, M. Superionic Conduction in Substoichiometric LiAl Alloy: An Ab Initio Study. *Phys. Rev. Lett.* **2009**, *103*, 125901. Dai, J.; Yuan, J. Large-scale efficient Langevin dynamics, and why it works. *EPL* **2009**, *88*, 20001.
- (52) Car, R.; Parrinello, M. Unified Approach for Molecular Dynamics and Density-Functional Theory. *Phys. Rev. Lett.* **1985**, *55*, 2471–2474.

- (53) Wu, Y.; Tepper, H. L.; Voth, G. A. Flexible Simple Point-Charge Water Model with Improved Liquid-State Properties. *J. Chem. Phys.* **2006**, *124*, 024503.
- (54) Lippert, G.; Hutter, J.; Parrinello, M. A Hybrid Gaussian Plane Wave Density Functional Scheme. *Mol. Phys.* **1997**, *92*, 477–487.
- (55) VandeVondele, J.; Krack, M.; Mohamed, F.; Parrinello, M.; Chassaing, T.; Hutter, J. Quickstep: Fast and Accurate Density Functional Calculations Using a Mixed Gaussian and Plane Waves Approach. *Comput. Phys. Commun.* **2005**, *167*, 103–128.
- (56) VandeVondele, J.; Hutter, J. Gaussian Basis Sets for Accurate Calculations on Molecular Systems in Gas and Condensed Phases. *J. Chem. Phys.* **2007**, *127*, 114105.
- (57) Goedecker, S.; Teter, M.; Hutter, J. Separable Dual-Space Gaussian Pseudopotentials. *Phys. Rev. B* **1996**, *54*, 1703–1710.
- (58) Krack, M. Pseudopotentials for H to Kr Optimized for Gradient-Corrected Exchange-Correlation Functionals. *Theor. Chem. Acc.* **2005**, *114*, 145–152.
- (59) Genovese, L.; Deutsch, T.; Goedecker, S. Efficient and Accurate Three-Dimensional Poisson Solver for Surface Problems. *J. Chem. Phys.* **2007**, *127*, 054704.
- (60) Kühne, T. D.; Krack, M.; Parrinello, M. Static and Dynamical Properties of Liquid Water from First-Principles by a Novel Car–Parrinello-like Approach. *J. Chem. Theory Comput.* **2009**, *5*, 235–241.